Using Local Correlation Tracking to recover solar spectral information from a Slitless Spectrograph

Hans T. Courrier*[a], Charles C. Kankelborg[a]
[a]Dept. of Physics, Montana State Univ./Bozeman, P.O. Box 173840, Bozeman, MT USA 59717-3840

ABSTRACT

The Multi-Order Solar EUV Spectrograph (MOSES) is a sounding rocket instrument that utilizes a concave spherical diffraction grating to form simultaneous solar images in the diffraction orders m = 0, +1, and −1. The large 2D field of view allows a single exposure to capture spatial and spectral information for large, complex solar features in their entirety.

Most of the solar emission within the instrument passband comes from a single bright emission line. The m = 0 image is simply an intensity as a function of position, integrated over the passband of the instrument. Dispersion in the images at m = ±1 leads to a field-dependent displacement that is proportional to Doppler shift. Our goal is to estimate the Doppler shift as a function of position for every exposure. However, the interpretation of the data is not straightforward. Imaging an extended object such as the Sun without an entrance slit results in the overlapping of spectral and spatial information in the two dispersed images.

We demonstrate the use of local correlation tracking as a means to quantify the differences between the m = 0 image and either one of the dispersed images. The result is a vector displacement field that may be interpreted as a measurement of the Doppler shift. Since two dispersed images are available, we can generate two independent Doppler maps from the same exposure. We compare these to produce an error estimate.

Keywords: instrumentation: spectrographs, space vehicles: instruments, Sun: UV radiation, techniques: imaging spectroscopy

1. INTRODUCTION

The MOSES instrument utilizes a concave spherical diffraction grating, blazed for m = +1, 0, and −1 spectral orders, to form images on three 2048 x 1024 rear-illuminated CCDs with 13.5μm pixels. Focal length is 4.74 m with an 8cm square aperture, the resulting FOV is 20" x 10." The ruling pitch of the grating yields a dispersion of 29 km/s (29 mÅ) per pixel. Multilayer coatings and thin film filters limit the instrument passband to a few spectral lines, the brightest of which is the Lyman alpha transition of He *II* at 30.4nm. A schematic of the grating and imaging detectors is shown in figure 1. The top, center, and bottom detector planes in figure 1 image the m = +1, 0, and −1 spectral orders respectively. The MOSES instrument is a stereoscopic imaging spectrograph and does not use an entrance slit[1]. The spatial axis is the same in all three spectral orders, however the direction of the dispersion axis is reversed between the m = ±1 orders. The images formed in these two orders are not symmetric. When imaging an object that has some spectral width, components that are redward of the instrument passband center (the letter "A" in figure 1) are shifted away from the m = 0 order CCD in the m = ±1 order images. Conversely, the blueward components of the object ("B" in figure 1) are shifted towards the m = 0 order CCD. There is no dispersion in the m = 0 order image.

While the images formed in all three orders are co-temporal, disentangling the spatial and spectral information that is encoded along the same axis in the outboard images is not straightforward. This is further complicated in the MOSES data in that each image order has a different set of optical aberrations associated with it. We perform the stereoscopic inversion by cross-correlating patches of the m = 0 and +1, and m = 0 and −1 order images[2] to determine the spatial shift between image pairs. The Fourier Local Correlation Tracking (FLCT)[3] routine is employed as a fast and efficient means of performing the cross-correlation and generating subsequent per pixel vector displacement fields for image pairs.

*hcourrier@physics.montana.edu; phone 1 406 994-3614; fax 1 406 994-4452; www.physics.montana.edu

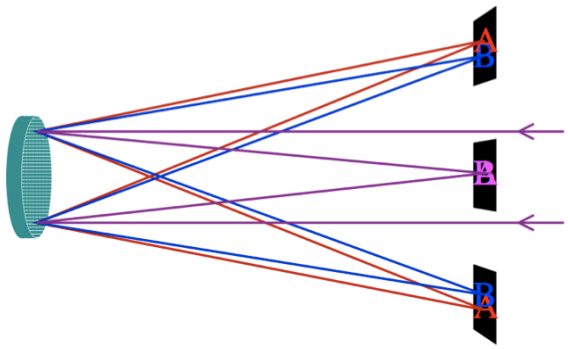

Figure 1. Schematic diagram of the MOSES instrument. Incident light on the right forms an undispersed image on the central m = 0 CCD. Dispersed images are formed on the outboard m = +1 and −1 CCDs.

In section 2, we prepare a synthetic data set that simulates MOSES flight data. We use this synthetic data to characterize the spatial and spectral response of the FLCT method in the context of a MOSES like data set. We use the results of section 2 and FLCT to generate dopplergrams of MOSES data collected during the Feb. 2006 flight[4] in section 3.

2. SYNTHETIC IMAGES

For the MOSES instrument, each of the three image orders has a different PSF associated with it that extends over several pixels. Small, isolated features in the 2006 flight data have allowed us to estimate a PSF for each image order.[5] Images of these PSF estimates are shown in figure 2, the contour is drawn at half maximum intensity and defines the size of the PSF. The three PSFs extend differently over several pixels along the horizontal (dispersed) and vertical (non-dispersed) axes, and it is this disparity in PSFs that drives the use of local correlation tracking to perform the stereoscopic inversion between image pairs. We are primarily interested in horizontal displacement between image pairs as this directly corresponds to Doppler shifts, but by also tracking the vertical displacement we can account for how the m = 0 order intensity PSF is mapped into each of the m = ±1 order images. This is demonstrated in figure 3a, displacement vectors are drawn from the m = 0 order PSF to the m = +1 order PSF. In figure 3b, displacement vectors are drawn from the m = 0 order PSF to the m = −1 order PSF. In figure 3a and 3b the centroids of the m = ±1 PSFs have been displaced horizontally by two pixels from the m = 0 PSF, which corresponds to a 58km/s red shift.

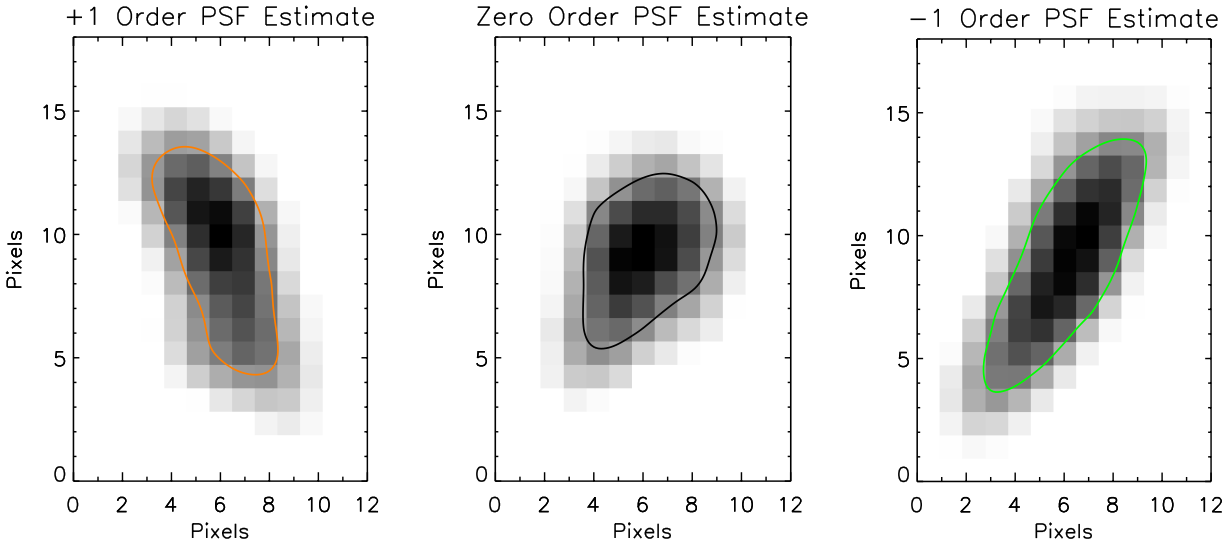

Figure 2. Estimates of the MOSES +1, 0, and −1, image order PSFs respectively. The contour is drawn at half maximum intensity for each image. Each PSF extends differently along the horizontal (dispersed) and vertical (non-dispersed) axes.

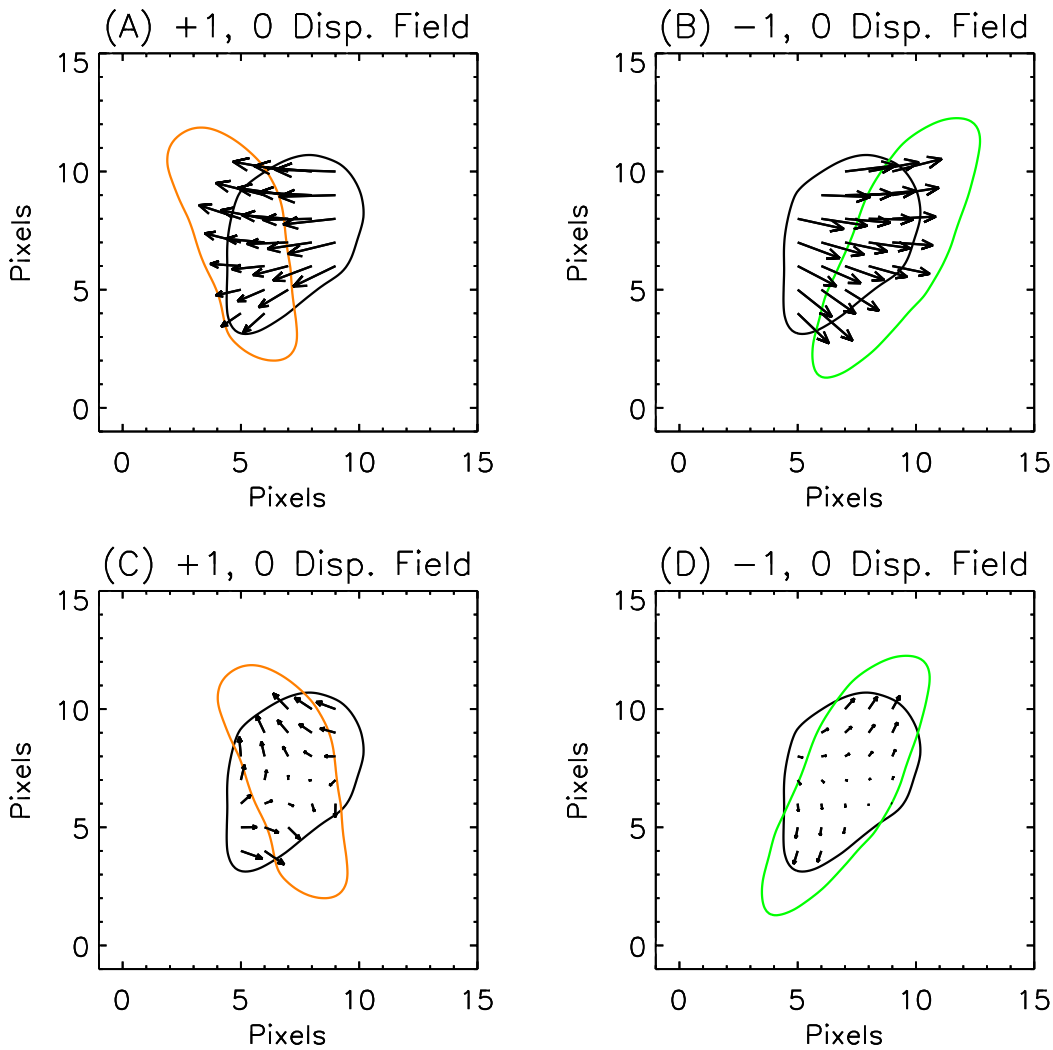

Figure 3. FLCT derived displacement vectors between the m = +1 and 0 (a, c) and m = −1 and 0 (b, d) image orders. Displacement vectors are plotted only for pixels contained within the m = 0 order PSF contour, and are in units of pixels. (a, b) Depict the centroid of the m = ±1 order PSF shifted 58km/s redward, corresponding to a two pixel translation leftward in (a) and rightward in (b). (c, d) PSF centroids are co-located, but the differing shape of the PSFs result in spurious red shifts near the top of the m = 0 PSF and blue shifts near the bottom.

We construct synthetic images to determine how well the FLCT method recovers spectral data from image pairs constructed with our PSF estimates. These synthetic images contain six test features designed to characterize the spectral and spatial response that FLCT is able to recover from the synthetic images. One pair of these features consists of horizontally adjacent red and blue shifted point sources, another pair vertically adjacent red and blue shifted point sources, one point source with non-zero (broadened) spectrum, and one point source with a non-dispersed spectrum. A synthetic image set consists of three images: one each for the m = 0, +1, and −1 orders. Since the m = 0 order image is not dispersed, spectral information is encoded into the m = ±1 images. This is accomplished by displacing each of the red and blue shifted point sources by one pixel (corresponding to a Doppler velocity magnitude of 29km/s) in the m = ±1 order images from their corresponding locations in the m = 0 order image. Test features for each image set are first convolved with the corresponding PSF estimate from figure 2, then placed in a noisy background with mean of 424 counts. Signal to background for the m = 0 image is ~2.9, similar to that of dim features in MOSES data.

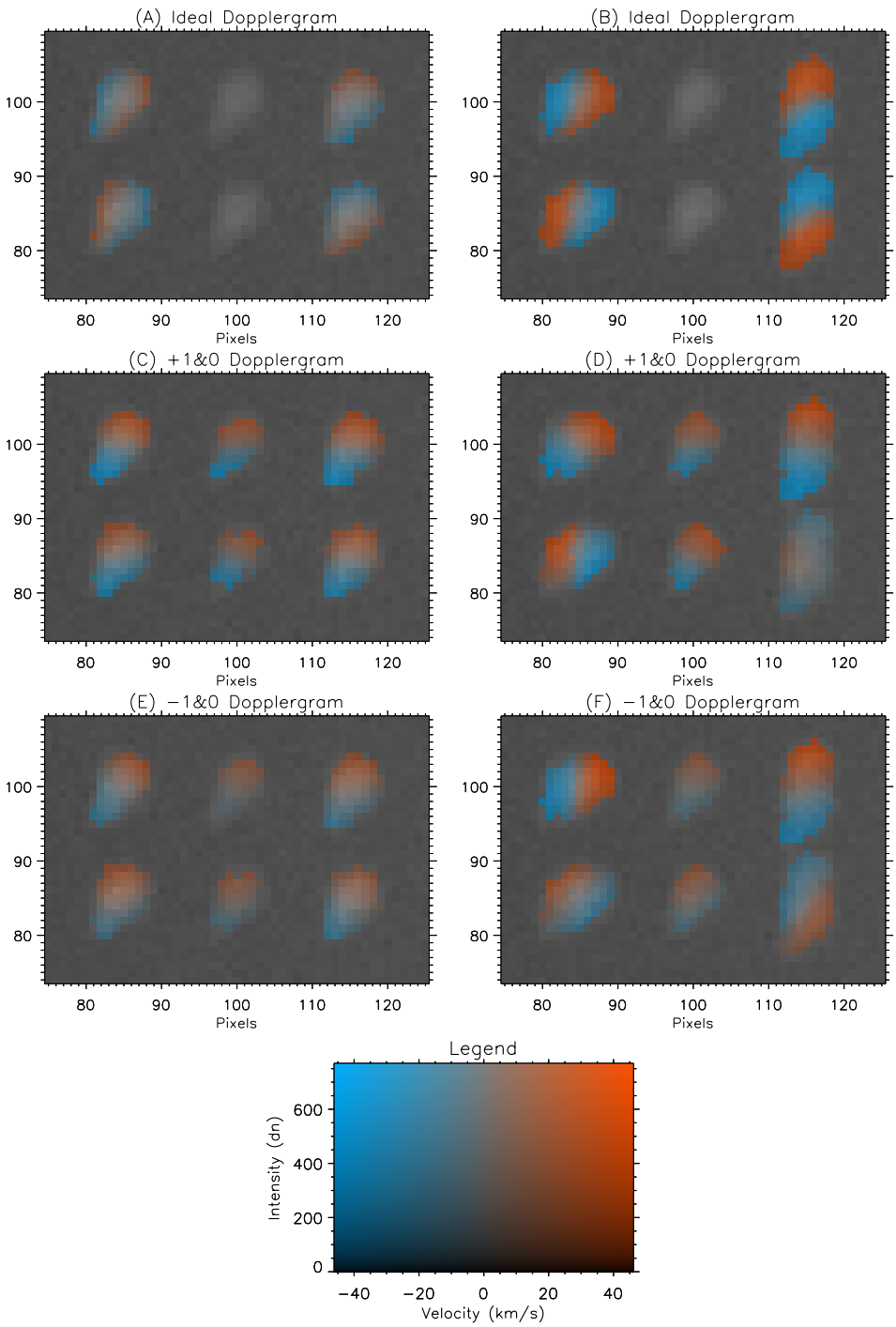

Figure 4. Dopplergrams generated from synthetic data, (a, b) depict the ideal dopplergram. Leftmost features in (a, b) are horizontally adjacent red and blue point sources, rightmost are vertically adjacent. Top center feature has non-zero spectral width, while the bottom center feature has no associated spectrum. Adjacent red and blue point sources in leftmost and rightmost features in each panel are displaced spatially by one pixel in (a) and three pixels horizontally (leftmost features) and five pixels vertically (rightmost features) in (b). (c, d) FLCT recovered version of (a, b) from m = +1 and 0 order images, (e, f) recovered from m = −1, and 0 order images.

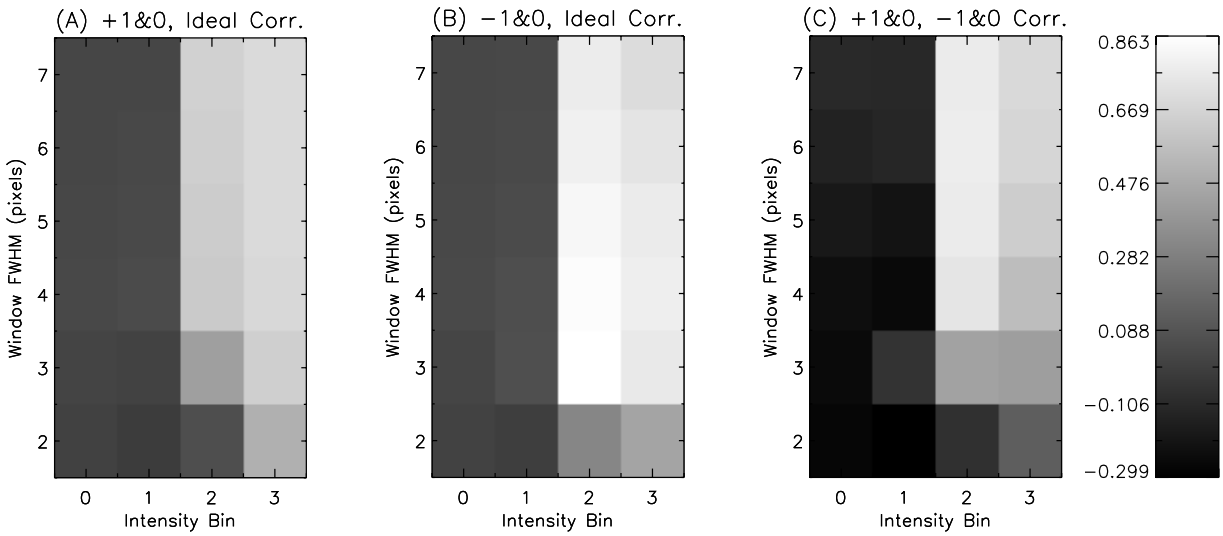

Figure 5. The Pearson correlation coefficient as a function of FLCT window size and intensity for (a) dopplergrams in figure 4b and 4d, (b) figure 4b and 4f, and (c) figure 4d and 4f. Intensity is binned into quartiles based on the m = 0 order image of figure 4b.

Dopplergrams derived from the synthetic images are displayed in figure 4, the velocity field is overlaid on the m = 0 order image as red and blue coloring indicating the intensity and direction of the Doppler velocities. The velocities are thresholded by binning the m = 0 order image counts into quartiles and ignoring those velocities corresponding to the dimmest quartile.

Figures 4a and 4b represent the ideal dopplergram for two different synthetic image sets. These two dopplergrams are derived from the known per pixel velocity field, $v(x,y)$, by

$$v'(x,y) = \frac{[I(x,y)v(x,y) \otimes \kappa]}{I(x,y) \otimes \kappa} \tag{1}$$

where $I(x,y)$ is the intensity of the m = 0 order image in counts, κ is the m = 0 order PSF estimate, and $v'(x,y)$ is the Doppler velocity field overlaid on the m = 0 order image. Figure 4a is the least resolved case, in this figure the horizontally adjacent (two features left side of panel) and vertically adjacent (two features right side of panel) are both displaced spatially by one pixel. For this displacement, red and blue point sources are so close together that the Doppler velocity cannot be distinguished near the centroid of these features. The top center feature has a spectrum with FWHM = 87mÅ centered around the instrument passband center, while the bottom center feature is non-dispersed. These two features are included as benchmarks since neither feature is associated with Doppler shifts, the non-dispersed feature because it has a singular spectrum, and the broadened feature because its spectral width is smaller than the width of the m = 0 PSF. In figure 4b the horizontally adjacent red and blue shifted point sources are displaced spatially by three pixels, the vertically adjacent point sources displaced by five pixels. The center two features are unchanged from those in figure 4a.

Dopplergrams in figures 4c and 4e are FLCT derived from the synthetic m = +1 and 0, and m = −1 and 0 order images, respectively, and correspond to the dopplergram of figure 4a. All of the test features in these two dopplergrams have similar structure. The center two features are red shifted at the top and blue shifted at the bottom, with features in figure 4c having larger magnitudes than those of 4e. These shifts are artifacts of the differing point spread functions of the image pairs as seen in the displacement fields of figure 3c and 3d. In figure 3c, the long axes of the m = +1 and 0 order PSF estimates are close to perpendicular when the centroids are co-located. This results in FLCT recovering red shifts near the top of the m = 0 order PSF and blue shifts near the bottom. The axes of the m = −1 and 0 are more closely aligned in figure 3d, red and blue shifts are still recovered but have smaller magnitudes than those of 3c. Comparing figure 3c to 4c, and figure 3d to 4d, the systematic error in Doppler velocities in figure 4c and 4d is well described by the

misalignment of the PSFs. The remaining four features of figure 4c and 4e all show similar structure as the central two features. This is because FLCT is not able to recover the spectral information for these features, the spatial separation between red and blue point source pairs is smaller than the PSF for all three image orders. To FLCT, these features appear to be no different than the non-dispersed feature.

The FLCT derived dopplergrams of figure 4d and 4f correspond to the ideal case of 4b. In figure 4f, FLCT is able reproduce much of the original velocity field structure but underestimates Doppler velocities for the bottom two red and blue shifted point source features. Errors in velocity and reproducing the structure of the bottom left feature are attributed to a combination of the alignment of the m = −1 and 0 order PSF and unfavorable (for this feature) dispersion direction of the m = −1 order image. Dispersion causes the PSFs of the red and blue shifted point sources to run together in the m = −1 order, confusing correlation of this feature. Figure 4d shows the FLCT dopplergram derived from the m = +1 and 0 order images. Errors in structure of the upper left feature are again a result of unfavorable dispersion direction, in this case of the m = +1 order. In both figure 4d and 4e, FLCT has difficulty in reproducing the lower right feature. This is largely due to the symmetry in how FLCT generates the displacement field between images. For a given pair of images, the displacement field from the m = 0 to m = +1 order image has the same magnitude but opposite sign as the field from the m = +1 to m = 0 order image. FLCT chooses to locate the displacement field vectors spatially somewhere in between the correlated features of each image pair. This would be appropriate for the intended purpose of FLCT: inferring the velocity field at an intermediate time between two ordinary images taken some time apart. For our application, it would be more appropriate to locate the displacement field at the source feature in the m = 0 order image, because feature positions in the two dispersed orders are displaced from their actual locations on the Sun according to the Doppler shift of the features. For the lower right feature in 4d and 4e, the red and blue shifted point sources are not separated enough so that the offset displacement fields generated by FLCT overlap, resulting in the failure to reproduce this feature.

The FLCT dopplergrams are largely dependent on the size of the patches used for the cross-correlation. The size of the patch used for cross-correlation effectively sets the scale size for the input images. Larger patches reduce artifacts due to the different PSFs associated with each input image, however spatial resolution is reduced[2]. In the FLCT routine, the size of the cross-correlation patch is determined by specifying the FWHM of a Gaussian windowing function to deemphasize parts of the image far from the pixel where the cross-correlation is calculated. The optimum size of the windowing function for our synthetic images is determined from figure 5. Correlation between each dopplergram of figure 4b, 4d, and 4f, (the resolved synthetic image set) is displayed as a function of m = 0 order image intensity (binned in quartiles) and windowing function size in pixels. There is little change in correlation for window sizes of five to seven pixels, selecting a window size of five pixels provides the best correlation between the m = +1 and 0, and m = −1 and 0 order dopplergrams. We use a window size of five pixels to generate dopplergrams from our synthetic images and MOSES data.

3. FLCT AND MOSES DATA

The MOSES instrument was launched February 8, 2006 from White Sands Missile Range, New Mexico. Over the course of approximately five minutes, twenty seven exposures were taken above 160km. Data from this flight have been dark subtracted, the outboard order images co-aligned to the central order, and optical distortion removed from all images. Intensities are in units of data numbers (DN) per second and normalized so that each image has the same mean DN/s as the exposure closest to apogee, the fourteenth exposure.[4] A dopplergram generated from the m = −1 and 0 orders of the twenty fourth exposure is shown in figure 6. Intensity has been binned in quartiles based on the m = 0 order image, with velocities corresponding the lowest intensity quartile not shown to threshold out noisy pixels. The color scheme of figure 6 has been scaled so that velocities of magnitude less than 50 km/s are visible, as the majority of the velocities of this dopplergram fall in the range between −50km/s and +50km/s. Velocities of magnitude greater than 50 km/s are plotted, but not distinguishable from those at 50 km/s. Groups of dark pixels in the FOV and the band of dark pixels across the left side and top of the image are a result of bad, missing, or saturated pixels in one or more image orders. Due to edge effects, velocities computed within the windowing size (five pixels) of bad pixels or image edges are considered unreliable.

The orange and green boxed areas of figure 6 are shown in greater detail in the left and right hand columns of figure 7, respectively. Dopplergrams 7a and 7b are generated from m = +1 and 0 orders, 7c and 7d from the m = –1 and 0 orders. Intensity is again binned in quartiles with velocities corresponding to the lowest quartile ignored. Doppler velocities for

both images reference the color bar at the bottom of their respective columns. These two features are well isolated and show characteristics similar to those seen in transition region explosive events.[4,6,7] The magnitude of the Doppler velocities are large enough that these two events are not a result of artifacts of the instrument PSFs.

The feature depicted in figure 7a and 7c is the same explosive event analyzed by Fox et al.[4,8] We are able to reproduce similar features to this analysis, with the core of the feature largely red shifted and centered between two blue shifted wings. Unlike the analysis by Fox et al, we resolve the upper wing as mostly blue shifted and only becoming red shifted towards the tip. The PSF marginally resolves details of this size. Comparing figure 7a to figure 5d and 7c to 5f, we see similar structure in the interface between the lower blue shifted wing and central core as that in the upper left feature of 5d and 5f. The structure of the interface between the core and the upper wing is less clear. There are some similarities to the lower right feature of figures 5d and 5f. The structure of the event depicted in figure 7b and 7d is less complex. This appears to be a largely blue shifted event, but has striking similarities to the lower right feature in figure 5d and 5f. Thus, while the blue shift is dominant in this feature, it appears that a red shifted component is also present.

Correlation between dopplergrams 7a and 7c, and dopplergrams 7b and 7d are plotted in figure 8a and 8b respectively. Correlation is again plotted as a function of FLCT window size and m = 0 order image intensity, binned into quartiles. We expect correlation to increase as window size increases, as a larger window size smoothes over the difference between image order PSFs. In figure 8, we see increasing anti-correlation as window size increases. The anti-correlation is likely a result of the symmetry of the displacement field generated by FLCT and the resulting ambiguity of its spatial location, as discussed in section 2.

4. DISCUSSION AND CONCLUSIONS

The MOSES instrument collects simultaneous EUV images in three spectral orders of a concave diffraction grating. Here we have demonstrated, on both synthetic and real data, the derivation of dopplergrams from image pairs using local correlation tracking. In section 2, we show the origin of systematic errors that mainly affect poorly resolved structures. These systematic errors are due to the differing PSFs of each image order. A PSF equalization procedure described by S. Atwood and C. Kankelborg, also in this volume, may reduce or eliminate the systematic Doppler shift errors documented in this paper.

It is also apparent from section 2 that FLCT does not correctly locate the Doppler shifts. This unfortunately hampers our quantitative, pixel-by-pixel comparison of the dopplergrams derived from the m = +1 and 0, and m = -1 and 0 image orders. It would be helpful to develop a similar (and possibly simpler) algorithm that places the Doppler shifts (displacement vectors) at the source locations in the m = 0 order image, rather than between the m = ±1 and m = 0 order images. Once this shortcoming is addressed, we expect to be able to better asses and improve our Doppler shift estimates by comparing and perhaps combining results gained from different image order pairs.

Applications of FLCT to actual MOSES data in section 3 show some promising results, despite the systematic errors documented in section 2. Strong events such as those shown in figure 7 look broadly similar whether the dopplergram is generated from the m = +1 and 0, or m = −1 and 0 order images. Comparing the features of figure 7 to the synthetic images of figure 5, it is clear that resolving the Doppler shifts of features this size is at or outside the limitations of our FLCT based method.

Moving forward, our strategy will be (1) develop a local correlation tracking algorithm that identifies the displacements with locations in the source image rather that between source and destination images; (2) Apply this algorithm to both synthetic and real MOSES data, as we have done in this study; (3) Develop quantitative pixel-by-pixel diagnostics, similar to the cross-correlations presented here, to estimate systematic errors and, to the extent possible, correct them.

ACKNOWLEDGEMENTS

This work is supported by the NASA Heliophysics Sounding Rocket Program, grant number NNX14AK71G.

REFERENCES

[1] Kankelborg, C. C., and Thomas, R. J., "Simultaneous Imaging and Spectroscopy of the Solar Atmosphere: Advantages and Challenges of a 3-Order Slitless Spectrograph," Proc. SPIE 4498, 16 (2001).

[2] Deforest, C., Elmore, D. F., Bradford, M. P., Elrod, J., and Gilliam, D. L., "Stereoscopic spectroscopy for efficient spectral imaging and magnetography," ApJ 616, 600-616 (2004).

[3] Fisher, G. H., and Welsch, B. T., "FLCT: A Fast, Efficient Method for Performing Local Correlation Tracking," PASP conf. series 383, 373 (2008).

[4] Fox, J. L., Kankelborg, C. C., and Thomas, R. J. "A Transition Region Explosive Event Observed in He II with the MOSES Sounding Rocket," ApJ 719, 1132-1143 (2010).

[5] Rust, Thomas, MSU Physics, private communication, Mar. 2015.

[6] Dere, K. P. "Bi-directional plasma jets produced by magnetic reconnection on the Sun," Adv. Space Res. 14, 13-22 (1994).

[7] Dere, K. P., Bartoe, J.-D. F., and Brueckner, G. E., "Explosive events in the solar transition zone," Sol. Phys. 123, 41-68 (1989).

[8] Fox, J. L., [Snapshot Imaging Spectroscopy of the Solar Transition Region: The Multi-Order Solar EUV Spectrograph (MOSES) Sounding Rocket Mission], Phd thesis, Montana State University, 126-132 (2011).

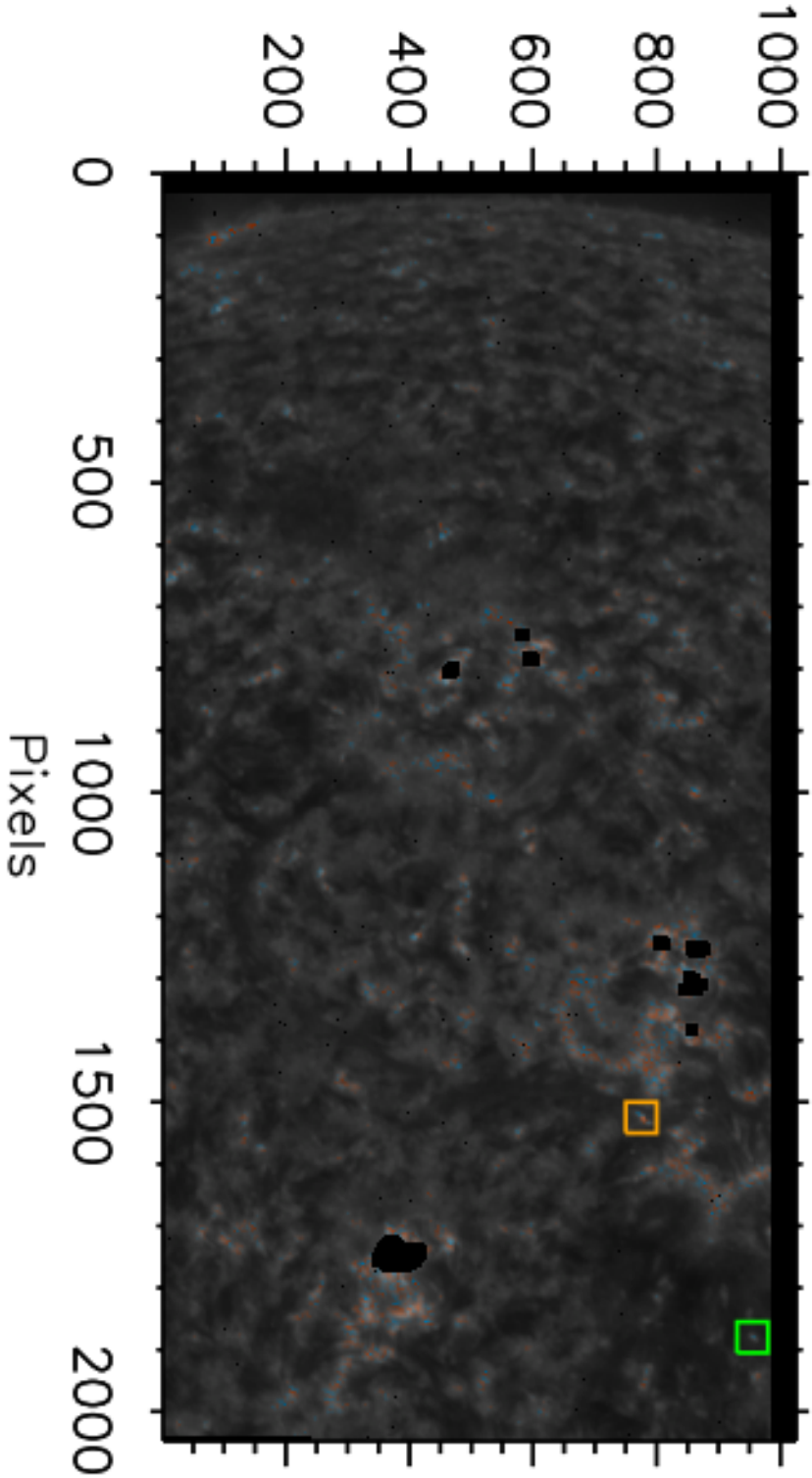

Figure 6. FLCT dopplergram of the twenty fourth MOSES exposure, generated from the m = −1 and 0 order images. Dark pixels are bad or missing data.

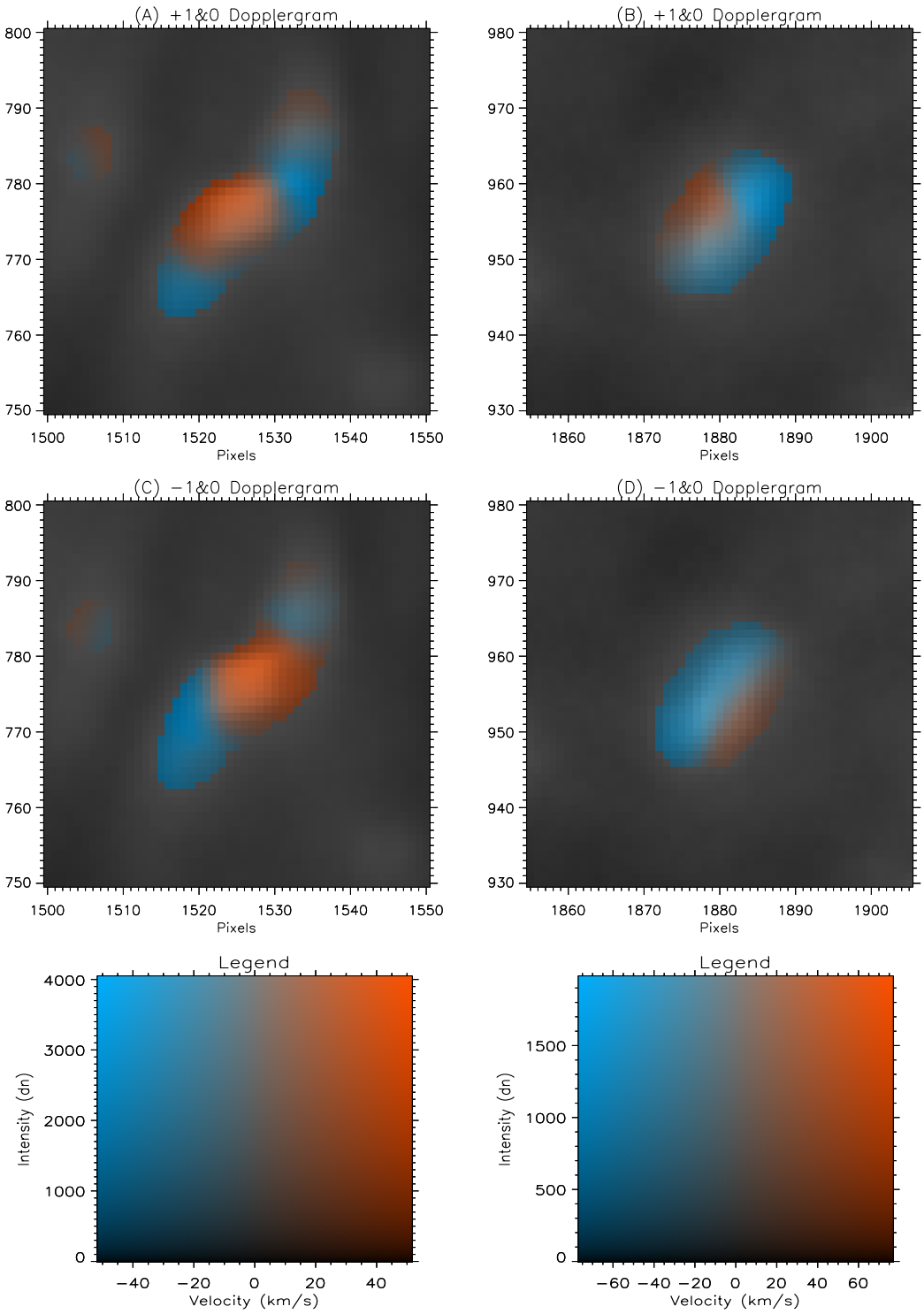

Figure 7. (a, c) Larger view of orange boxed area of figure 6. (b, d) Larger view of green boxed area of figure 6. Dopplergrams are thresholded by binning intensity of the m = 0 order image into quartiles and ignoring velocities corresponding to the dimmest quartile to remove noise pixels.

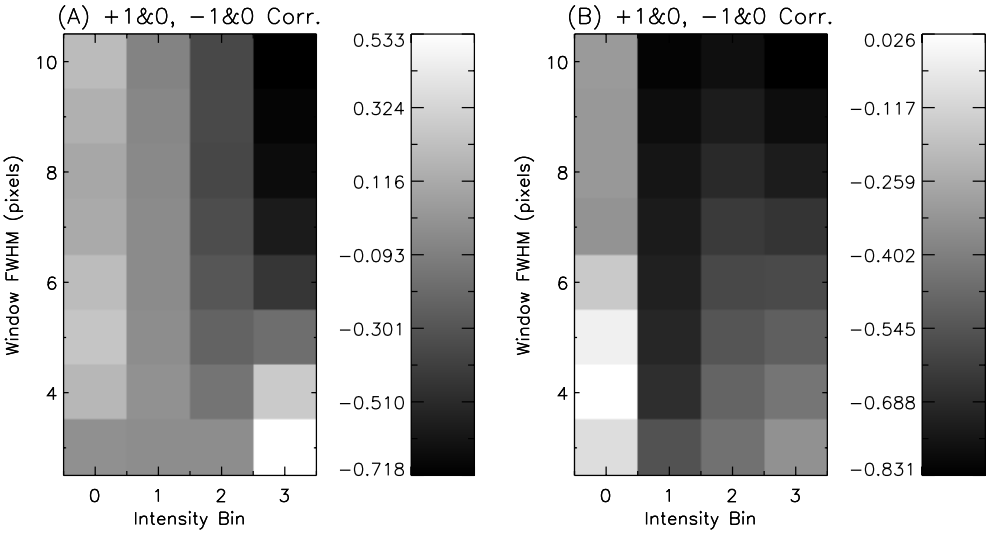

Figure 8. Correlation as a function of FLCT window size and intensity for (a) dopplergrams in figure 6a and 6c, and (b) dopplergrams in figure 6b and 6d.